九州大学大学院総合理工学報告
第28巻 第1号 1-8頁 平成18年6月

Engineering Sciences Report, Kyushu University
Vol.28, No.1 pp.1–8, JUN. 2006

Thermocapillary convection in a shallow annular pool of silicone oil

Wanyuan Shi[*1,2] and Nobuyuki Imaishi[*3,†]
[†] E-mail of corresponding author: imaishi@cm.kyushu-u.ac.jp

(Received April 25, 2006)

Thermocapillary flow in a shallow annular pool (R_i=20 mm, R_o=40 mm and depth d=1.0 mm) of silicone oil (0.65 cSt, Pr=6.7), heated from the outer wall and cooled at the inner wall, is investigated by numerical simulation. Numerical results clarified details of pattern formation and oscillatory behavior of hydrothermal waves (HTW) as well as the critical conditions for their incipience. In non-rotating pool, the critical Marangoni number Ma_c for the incipience of the HTW is 8.396×10^3(ΔT_c=5.03K). The critical azimuthal wave number m_c is 27. At slightly super critical conditions, a single group of HTW propagating in the azimuthal direction is dominant after a long calculation time. Further increase in Ma causes coexistence of several groups of HTW with different wave numbers and propagation directions. Effect of a slow rotation of the pool around its central axis destabilizes the basic steady axisymmetric flow against HTW. At Ta=0.322 (corresponding to a rotation rate of 2 r.p.m.), the Ma_c was determined as 8.096×10^3 (ΔT_c=4.85K) with m_c=30. Over a range of Ma from 8.76×10^3 to 2.0×10^4, numerical simulations indicate that the HTW propagates azimuthally opposite to the direction of the pool rotation in a rotating coordinate. This phenomenon, i.e. a selection of propagation direction, is caused by the azimuthal velocity component in the basic flow field induced by the Coriolis force. At Ma=1.34×10^4, the azimuthal wave number m increases up to 54 accompanied by an appearance of finger-shaped patterns. At Ma=2.0×10^4, two groups of HTW with greatly different wave numbers (m=48 and m=5) coexist and propagate in the opposite azimuthal directions.

Keywords: Hydrothermal wave, thermocapillary convection, rotation, numerical simulation, silicone oil, pattern formation

1. Introduction

In past few decades, thermocapillary convection had been increasingly interested in many fields, such as subcooled nucleate pool boiling [1-3], thin-film coating [4], and melt growth of single crystals [5-6]. In single-crystal growth processes, such as the Czochralski (Cz) methods, thermocapillary force gives significant effects on the stability of melt flow [7-9]. Spatio-temporal changes of the unstable melt flow cause inhomogeneous distribution of dopant and point defects in the grown crystals. In Cz melt pools, convection is driven by buoyancy force, thermo-capillary force, centrifugal force and Coriolis force. Combination of these driving forces sometime leads very much complex and unstable flow patterns accompanied by time-dependent three dimensional oscillations of temperature and concentration fields [10]. Spoke patterns on oxide melt surfaces are explained by the Marangoni effect caused by a temperature gradient perpendicular to the liquid surface (Marangoni instability of Pearson type) [7-8]. However, Azami et al. suggested the hydrothermal wave type instability (caused by a horizontal temperature gradient on the surface) is a possible mechanism of pattern formation in shallow pool of silicon melt in a Cz furnace based on their experiment [10].

The hydrothermal wave (HTW) type flow instability was first predicted by Smith and Davis (hereafter SD) [11]. They investigated stability of thermocapillary flows in rectangular shallow pool of liquid induced by a horizontal temperature gradient on the surface and found a new type of oscillatory instability on the basis of three-dimensional, time-dependent linear stability analysis (LSA).

In rectangular pools, this type of flow instability had been confirmed by experiments using various silicone oils with different Prandtl numbers [12-16]. To eliminate the effects of buoyancy, experiments were conducted mostly in shallow liquid layers. Riley and Neitzel [13] and Burguete et al. [14] obtained a stability limit diagram for thermocapillary flow as a function of liquid depth. Their results suggested that the critical Marangoni number ($Ma^*=\gamma_T\Delta T d^2/\mu\alpha L$) increases with liquid depth d, where γ_T is the temperature coefficient of surface tension [13].

Thermocapillary flow instability in annular liquid pools had been studied by several researchers. Kamotani et al. [17-19] conducted a large set of microgravity experiments on oscillatory thermo-capillary flow of silicone oil in open cylindrical containers with aspect ratios ($As=(r_o-r_i)/d$) close to 1 or 2 (with cylindrical diameters of 12, 20 and 30 mm) where liquid was heated by a hot solid cylinder located at the pool axis or a laser beam. They observed two or three lobed surface temperature patterns.

[*1] Interdisciplinary Graduate School of Engineering Sciences, Kyushu University, Japan
[*2] College of Power Engineering, Chongqing University, China
[*3] Institute for Materials Chemistry and Engineering, Kyushu University, Japan

Mukolobwiez et al. [20] observed HTW traveling in the azimuthal direction in a shallow annular channel of silicone oil (Pr=10) (1.7 mm in depth, 10mm in width with a mean radius 80 mm) heated from the inner wall. The influence of liquid depth on the wavelength of the HTW was investigated by Schwabe et al. [21] through their experiments on thermocapillary flow in annular liquid pools of ethanol (Pr=17) with thickness ranging from 0.6 mm to 3.6 mm (inner radius 20mm, outer radius 77mm), heated at the inner rod. They observed short wavelength temperature patterns with curved arms (part of spirals) in shallow liquid pools (d<1.4 mm) and long-wavelength temperature patterns in deeper pools (d>1.4 mm). Hoyas et al. [22, 23] conducted linear stability analysis and obtained a stability diagram for the incipience of oscillatory flow in annular liquid pools heated at the inner wall (aspect ratio $2.5 \le As \le 10$), taking the surface heat transfer to the ambient air into account.

For annular pools heated at the outer wall and cooled at the inner wall, Garnier and Chiffaudel [24] clearly observed HTWs with spiral-like arms in an annular container of silicone oil (Pr=10, 135mm in diameter with an inner cold rod of 8 mm in diameter, and with a depth of 1.2 mm or 1.9 mm; As=52.9 or 33.4). They observed pulsating, target-like wave patterns (i.e., coaxial circles traveling outward in the radial direction) dominant only near the cold inner wall, as well as the curved arms of HTW dominant in the whole area of the liquid pool. Later, Schwabe et al. [25, 26] found that gravity significantly stabilizes the basic steady radial thermocapillary flow of silicone oil (Pr=6.8), by comparing their results of on-ground experiments and microgravity experiments on the FOTON-12 satellite.

Since it is difficult to understand the details of thermocapillary convection through experiments, numerical simulations had been carried out by some researchers. Xu and Zebib [27] conducted a set of numerical simulations of thermocapillary convection in a rectangular pool and obtained a stability diagram and wave numbers. Thermocapillary flow in an annular pool of silicone oil was worked out by Sim et al. [28] for the same geometry as that of Schwabe's experiment on FOTON-12. On the other hand, Li and coworkers [29] also conducted numerical simulations of thermocapillary convection in annular pools with the same geometry as those of the FOTON-12 experiments. Their stability diagram was compared with those of FOTON-12 microgravity experiments. Recently, Shi and Imaishi [30] conducted a set of numerical simulations for silicone oil (Pr=6.7) in an annular container with the same geometry as that of Schwabe's experiment [26] but much thinner depth (d=1mm, As=20) and evaluated the effect of gravity on the critical Marangoni number and wave patterns.

Effects of the Coriolis force on the critical condition for the incipience of hydrothermal waves were analyzed in order to evaluate the effect of system rotation (order of the rotation rate Ω is about 10^{-3} rad/s) during the microgravity experiments in space vehicles orbiting around the earth with a period of 2 hours or so. Zebib [31] conducted a linear stability analysis of thermocapillary convection in an infinitely extended rectangular pool. His results indicate the effect of system rotation on the incipience of three dimensional secondary flows over a wide range of the Taylor number ($Ta=\Omega d^2/\nu$) between –50 to 100. For rotation around an axis perpendicular to the liquid surface, Zebib's LSA predicts that the basic flow is slightly stabilized against HTW but destabilized against stationary three dimensional disturbances if Pr number is smaller than a critical value, Pr_c, which depends on Ta, such as Pr_c=1 for Ta=3 and Pr_c=7.1 for Ta=5, respectively. At Ta=8, HTW disappears and the basic flow becomes unstable against stationary 3D disturbances at much smaller Ma_c than those of SD. Further increase in Ta increases the critical Marangoni number. At $Ta \ge 50$, the basic flow is stabilized compared with SD in the whole range of Pr against stationary disturbances. Bauer and Eidel [32] analyzed the axisymmetric thermocapillary flow (the basic flow) in deep cylindrical containers similar to the microgravity experimental apparatus used by Kamotani, heated at the outer wall under gravity and rotating about its center axis over a range of $Ta^*=\Omega a^2/\nu$ = 1 - 400 (here, a is the radius of the outer cylinder). The Coriolis force induces an azimuthal velocity in a rotating annular pool. The azimuthal velocity near the free surface is large and directs in the same direction as that of the pool rotation. Far below the free surface, the azimuthal velocity is small and directs opposite to that of the pool rotation. Sim and Zebib [33] numerically investigated the effect of orbiting motion of the space vehicle on the transition to an oscillatory flow from the basic thermocapillary convection in an open deep cylindrical annulus heated from the inner wall with As=1.0 and Pr=30, exactly corresponding to Kamotani's microgravity experiments. They found that Ma_c decreases with increasing Taylor number in a range of Ta= 0 - 10.

However, there are few numerical reports on the HTW in very thin annular pools of silicone oil, such as 1.0 mm. In this work, we numerically investigate the thermocapillary convection and the effects of the pool rotation (Ta) on the basic thermocapillary flow and the critical conditions for the incipience of hydrothermal waves in a shallow annular pool of silicone oil heated from the outer wall. The value of Taylor number in this work Ta=0.322 (rotating rate of 0.21 rad/s) is much smaller than those in the literatures [31-33].

2. Model and methods

2.1 Physical and mathematical models

As shown in Fig.1, the model system is an annular pool with an open top free surface and a solid bottom, with an inner solid wall (radius R_i=20 mm), an outer wall (radius R_o=40 mm) and depth d=1.0 mm. These geometries are same as those of Schwabe's experimental apparatus [26] except for the liquid depth. The pool can rotate around the vertical central axis with constant rotating rate. The fluid is silicone oil. Its physical properties are listed in Table 1.

The outer wall is maintained at a constant temperature T_h while the inner wall at a lower temperature T_c (T_h>T_c and ΔT=T_h-T_c). Top and bottom surfaces are considered to be adiabatic. The silicone oil is regarded as an incompressible Newtonian fluid with constant properties except for the temperature dependence of surface tension. The Marangoni effect (thermocapillary force) acts on the surface. The flow is considered to be laminar. The liquid top surface is assumed to be flat and nondeformable.

Under the above assumptions, a mathematical model is expressed by the following nondimensional equations in a coordinate system co-rotating with the pool around the z axis. In the cases of axisymmetric steady simulations, we assume that all gradients in the azimuthal direction are zero.

$$\nabla \cdot \boldsymbol{V} = 0 \tag{1}$$

$$\frac{\partial \boldsymbol{V}}{\partial \tau} + \boldsymbol{V}\cdot\nabla\boldsymbol{V} = -\nabla \boldsymbol{P} + \nabla^2 \boldsymbol{V} - 2Ta\,\boldsymbol{e}_z \times \boldsymbol{V} \tag{2}$$

$$\frac{\partial \Theta}{\partial \tau} + \boldsymbol{V}\cdot\nabla\Theta = \frac{1}{Pr}\nabla^2\Theta \tag{3}$$

Here, $\boldsymbol{e}_z$ is a unit vector in z direction. The followings are used for the boundary conditions.

At the top surface:

$$\frac{\partial u}{\partial z} = -\frac{Ma}{Pr}\frac{\partial \Theta}{\partial r},\quad \frac{\partial v}{\partial z} = -\frac{Ma}{Pr}\frac{\partial \Theta}{r\partial \theta}, \tag{4a, b}$$

$$w = \frac{\partial \Theta}{\partial z} = 0. \tag{4c,d}$$

At the bottom:

$$u = v = w = 0,\quad \frac{\partial \Theta}{\partial z} = 0. \tag{5a, b, c, d}$$

At the inner wall:

$$u = v = w = 0,\quad \Theta = 0. \tag{6a, b, c, d}$$

At the outer wall:

$$u = v = w = 0,\quad \Theta = 1. \tag{7a, b, c, d}$$

Initial conditions are as follows.

For axisymmetric steady simulations,

$$\boldsymbol{V} = 0,\quad \Theta = \frac{\ln\left(r/r_i\right)}{\ln\left(r_o/r_i\right)}. \tag{8a, b}$$

For 3D simulations, either Eqs. 8a, b, or a 3D results obtained at a smaller Ma was used as an initial condition. While for the simulations to determine Ma_c, axisymmetric steady fields obtained by axisymmetric simulation under the same Ma were used.

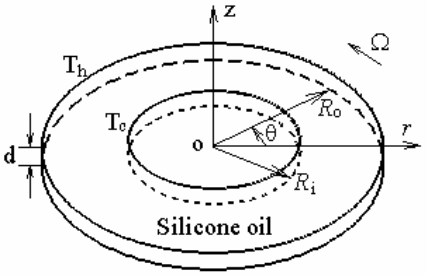

Fig.1 Configuration of the model system.

Table 1 Physical properties of silicone oil

Prandtl number, Pr=6.7
Density, ρ=760 kg/m^3
Thermal diffusivity, α=9.7×10^{-8} m^2/s
Kinematic viscosity, ν=6.5×10^{-7} m^2/s
Thermal expansion coefficient, ρ_T=1.34×10^{-3} 1/K
Temperature coefficient of surface tension, γ_T=8.0×10^{-5} N/m K

Here, u, v and w are velocities in r, θ and z directions, respectively. The length, time τ, pressure P, velocity and phase (angular) velocity ω of HTW are scaled by d, d^2/ν, $\nu\mu/d^2$, ν/d and ν/d^2, respectively. Non-dimensional temperature is defined as Θ=(T-T_c)/ΔT, here ΔT=T_h-T_c. The Marangoni, Prandtl and Taylor numbers are defined as Ma=$\gamma_T d\Delta T/\mu\alpha$, Pr=ν/α, Ta=$\Omega d^2/\nu$, respectively. Here, μ is the viscosity, γ_T=-$\partial\gamma/\partial$T the temperature coefficient of surface tension, γ the surface tension, and α the thermal diffusivity of silicone oil. Ω is the angular velocity of the pool rotation. The stream function ψ is defined as $u = -\frac{1}{r}\frac{\partial \psi}{\partial z}$, $w = \frac{1}{r}\frac{\partial \psi}{\partial r}$.

2.2 Numerical methods

The equations (1)-(8) were discretized by the control volume method in the staggered grid system. The non-uniform grids are constructed to achieve finer meshes in the regions near the free surface and bottom and also near the sidewalls where the boundary layer develops. The space intervals between two neighbor grids were changed in a sinusoidal function within a half cycle to provide finer grids near the boundaries. For example, in a mesh system with grid points of $202^r\times603^\theta\times21^z$, the minimum space intervals in the radius and z direction were 0.015 and 0.013, respectively. The azimuthal direction has uniform staggered grids in all cases. The central difference approximation was introduced for the diffusion terms. Convective terms were treated by the second-order upwind scheme excepted for the azimuthal direction where the QUICK scheme was adopted. The equations were discretized by a fully implicit method in the time marching. The

SIMPLEC algorithm [34] was used to handle the pressure coupling. The preconditioned Bi-CGStab algorithm [35] was applied to solve the discretized equations. Convergence at each time step was assumed when both of the following conditions were satisfied:

$$|R^i|_{\max} \le 10^{-N} \quad \text{and} \quad \left|\frac{\phi^{i+1}-\phi^i}{\phi^{i+1}}\right|_{\max} \le 10^{-4},$$

where $|R^i|_{\max}$ is the absolute maximum residual of the nondimensional continuity equation among all control volumes in ith iterating step. ϕ indicates any one of the variables u, v, w and Θ. N was varied between 12 and 10 depending on Ma i.e., N=12 was used for a small Ma and N=10 for a larger Ma. The numerical simulations were conducted on one PE of Fujitsu VPP5000/64 supercomputer at the Computing and Communications Center of Kyushu University.

The grid convergence was carefully checked through numerical simulations using different grid systems[30]. These results confirm the grid convergences. In order to save computation time, most of the following results were obtained using a grid $202^r \times 363^\theta \times 16^z$ for non-rotation pools. However, the critical Marangoni number and the critical frequency were determined on the basis of the results using a grid system of $202^r \times 603^\theta \times 16^z$. In the rotating pool, due to larger azimuthal wave number, a finer mesh $202^r \times 603^\theta \times 21^z$ was used to provide higher spatial resolutions. The grid convergence in a rotating case is shown in Table 2.

Table 2 Mesh dependency of the oscillatory parameters under Ma=1.0×10^4(ΔT=6.0K), Ta=0.322.

Mesh sizes (r×θ×z)	Wave number m	Frequency f (Hz)
202×603×16	27	0.547
202×603×21	30	0.547
202×723×21	30	0.547

3. Results in a non-rotating pool

3.1 The basic axisymmetric steady flow

In this system, a horizontal temperature gradient is imposed on the fluid in the radial direction, thus the thermocapillary flow arises at any finite value of Ma. When Ma is small, the thermocapillary flow is 2D steady and axisymmetric, called as the "basic flow". Numerical simulation results with small values of Ma are shown in Figs.2-4. Fig.2 shows the radial distribution of the surface temperature at two different ΔT. Thermal boundary layers appear near the inner and outer walls. With increase of Ma (ΔT), the surface temperature gradient (∂T/∂R) in the mid area increases. Fig.3-a shows the radial velocity u on

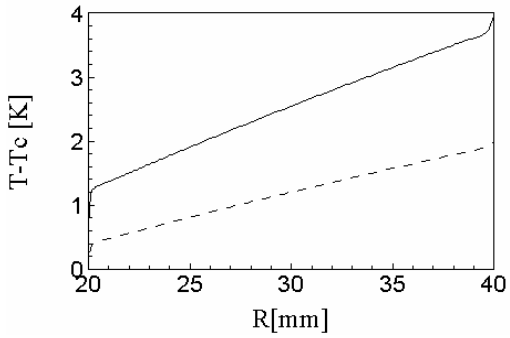

Fig.2 Surface temperature distributions as a function of radius R. Dashed line: ΔT=2.0 K. Solid line: ΔT=4.0 K.

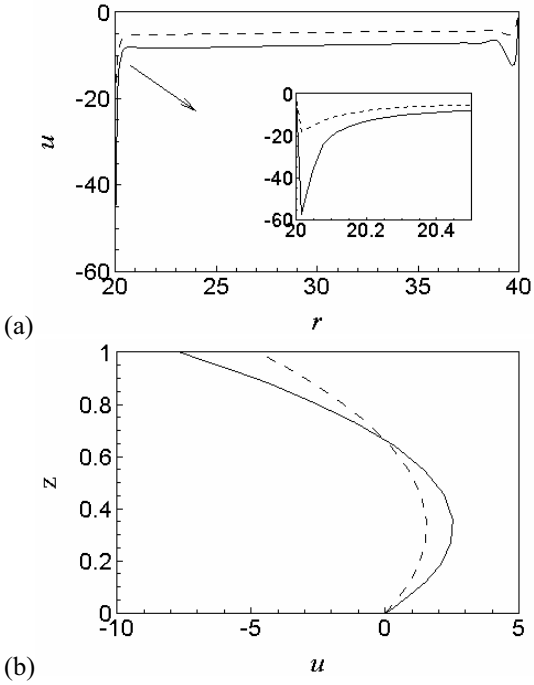

Fig. 3 Axisymmetric steady flow. (a). The radial velocity component profiles versus radius r on the surface. (b) The radial velocity component profiles versus axis z at r=30. Dashed line: Ma=3.34×10^3 (ΔT=2.0 K). Solid line: Ma=6.68×10^3 (ΔT=4.0 K).

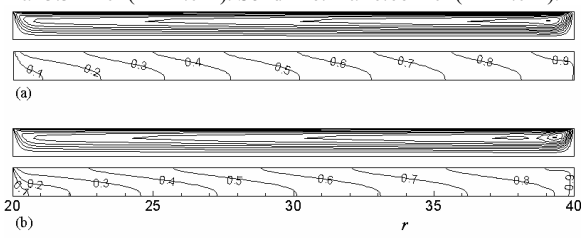

Fig.4 Streamlines and isotherms of the basic flow.
(a). Ma=3.34×10^3, ψ_{min}=-26.47, ψ_{max}=0.013.
(b). Ma=6.68×10^3, ψ_{min}=-49.63, ψ_{max}=0.029.

the surface as a function of r. The radial velocity increases with increase in Ma due to the larger radial temperature gradient on the surface. The radial velocity u at r=30 is shown in Fig. 3-b as a function of z. These profiles are similar to those of thermocapillary flow in a rectangular pool[11]. Fig. 4 shows the stream function and isotherms. It should be noted that there appears a strong roll cell near the hot wall driven by the large surface temperature drop there. In contrast, a very large temperature drop near

the cold inner wall causes a large surface velocity peak near the cold wall, followed by a steep deceleration down to zero at the cold wall as shown in Fig. 3-a.

As *Ma* increases, a second roll cell is induced next to the strong roll cell near the hot wall. However, for the steady basic flow in this pool the maximum number of the roll cells is two. If we conduct 2-D simulations under much larger *Ma* values, 2-D flow field becomes oscillatory and 7 or 8 roll cells are propagating in the radial direction from the cold wall to the hot wall.

3.2 Critical conditions for the incipience of HTW

As *Ma* exceeds a certain threshold value, the flow becomes unstable and oscillations start. The flow is 3D oscillatory. In the early period of the simulations, local radial velocities and local temperatures indicate temporal oscillations with very small amplitudes. These oscillations increase their amplitude exponentially with time following Eq. (9), as described in our previous paper [30].

$$X(\tau) = X_0 \exp[(\beta + i2\pi f^*)\tau] \qquad (9)$$

The nondimensional frequency of oscillations f^* is defined as $f^* = f d^2/\nu$, where f [Hz] is oscillation frequency of local values.

For each value of *Ma*, we can determine the growth rate constant β as a slope of a plot of the logarithm of a local value of surface velocity as a function of τ. A plot of β vs. *Ma* determines the critical Marangoni number for the incipience of 3D oscillatory flow as the *Ma* at which β becomes zero, since the state β=0 corresponds to a marginal stability limit. The wave number and phase velocity obtained by a simulation conducted at a *Ma* close to Ma_c are regarded as the critical wave number and critical phase velocity. Thus determined critical conditions are: Ma_c=8.396×10^3 (ΔT_c=5.03K), m_c=27 and f_c^*= 0.93. These are consistent within 2% of errors with the results by LSA [36].

3.3 HTW patterns

In order to express spatial distributions of oscillatory variables, we introduce the "fluctuation of X" for the 3D case, δX_3, where X stands for local temperatures, velocities and other parameters. δX_3 is defined as a deviation of a local value from its average value (averaged over the azimuthal direction), given by

$$\delta X_3(r,\theta,z,\tau) = X(r,\theta,z,\tau) - \frac{1}{2\pi}\int_0^{2\pi} X(r,\theta,z,\tau)\mathrm{d}\theta . \qquad (10)$$

Thus defined fluctuation of surface temperature clearly shows that surface temperature pattern (HTW), as shown Fig.5a. Generally, in the early periods of calculation, several groups of HTW originate at several locations and propagate in different directions. Number of HTW groups decreases with the progress of computation. However, two groups of HTW, with the same wave number but opposite azimuthal propagating directions, coexist for a considerably long time but gradually one of them becomes weaker. After a long time of calculation, at t=1140 s, only one group of HTW is dominant, as shown in Fig. 5a. A spatiotemporal diagram (STD: a plot of $\delta\Theta_{3\,(r=25,\,\theta,\,z=1,\,\tau)}$ over a time span of 10 seconds) indicates the propagation speed and counterclockwise traveling direction of these patterns as shown in Fig. 5b. These surface temperature patterns with curved arms are approximately expressed as $A_{(r)}\sin[m(\omega\tau+\theta+\varphi_{(r)})]$. Here, A is the amplitude of the temperature fluctuation, m the azimuthal wave number, $\omega = 2\pi f^*/m$ the phase velocity of the wave propagation in the azimuthal direction and φ the phase shift angle. A and φ are function of r. In cases with small *Ma*, the HTW patterns are clearly observable only in the inner part of the pool, being faded in the outer region. As *Ma* increases, HTW becomes dominant over the whole area of the liquid surface.

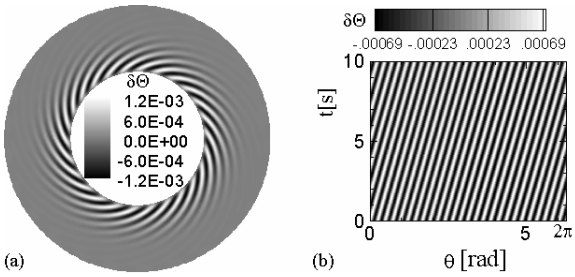

Fig. 5 Snapshot of the surface temperature deviation pattern when Ma=1.0×10^4 (ΔT=6.0K). Azimuthal wave number m=26.
(a). Surface temperature fluctuation (HTW).
(b). STD of $\delta\Theta$ at r=25 on the surface.

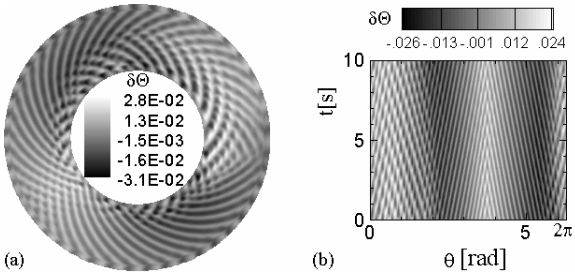

Fig.6 Surface pattern of the temperature deviation (a) and its STD (b) at r=30, Ma=2.0×10^4(ΔT=12.0 K).

Simulation with a larger *Ma*, such as Ma=2.0×10^4(ΔT=12.0 K), indicates several groups of HTW with different wave numbers coexisting in the pool with different traveling directions throughout the simulation ($t \le$ 1000s), as shown in Fig.6. Typical values of the wave number are m=28 for the HTW dominating near the inner wall and m=46 for the HTW dominating in the outer region. The coexistence of different groups of HTW is also

reported by Garnier et al. [24] although his pool geometry is different from that of the present system. However, we did not observe "targetlike (coaxial) waves" (m=0) propagating outward in the radial direction, which were reported by Garnier and Chiffaudel [24] near the inner wall of his annular pool which has much larger outer wall and smaller inner wall radiuses (67.5 mm×4 mm). The larger inner wall radius in the present system could produce smaller surface temperature gradient near the inner wall than its critical value for the incipience of the target-like waves.

A set of simulations with different values of Ma, ranging from 1.0×10^4 to 3.0×10^4, reveals that a single mode HTW occurs and their wave number slightly increases with Ma in a slightly super critical region. However, multi-mode patterns, such as shown in Fig. 6, appear at higher Ma range.

4. Effects of pool rotation

4.1 Basic flow in a rotating pool

If Ma is less than a certain threshold value, the thermocapillary flow in a rotating pool with Ta=0.322 (Ω=0.21rad/s in the anticlockwise direction) is steady and axisymmetric. Numerical results indicated that such a slow pool rotation gives practically no influence on the basic temperature and radial velocity distributions. However, there appears an azimuthal velocity component v in the pool. Fig. 7 shows a radial distribution of v on the surface and also a v profile in z direction at r=30. Since both the depth and rotation rate are small, the induced azimuthal velocity is positive in almost whole part of the liquid pool, except in limited areas near the bottom close to the outside wall, not shown in the figure.

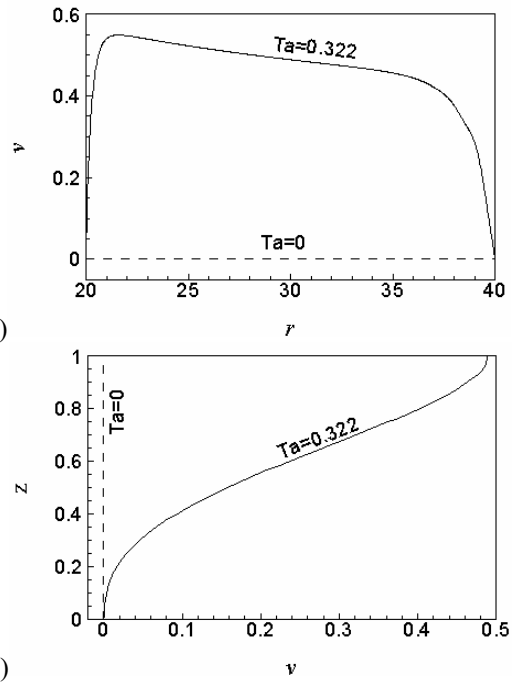

Fig.7 Azimuthal velocity distributions for Ta=0.322, Ma=8.35×10^3 (ΔT=5.0K). (a) radial distribution of v on the surface. (b) profile of v in z direction at r=30.

4.2 Critical conditions for the incipience of HTW

If Ma exceeds a certain threshold value, the basic flow can't keep its steady state against HTW. A set of numerical simulations with Ta=0.322 determined the critical conditions for the incipience of the HTW as Ma_c=8.096×10^3 (ΔT_c=4.85K), m_c=30 and ω_c=- 0.176. These are consistent with the result of LSA [36] within errors of less than 1%. It should be noted that the negative value of ω_c indicates the HTW propagates in the clockwise direction, i.e., in the opposite direction to the pool rotation. The propagation phase velocity in a co-rotating coordinate system is ω=-0.176 and the pool rotation angular velocity is Ta=0.322. Thus, if observed from a fixed point, the HTW pattern is rotating in the anticlockwise direction with a phase velocity of 0.146.

It can be seen that in a rotating pool, the Ma_c is 3.6% smaller than that of non-rotating case. This implies that the pool rotation destabilizes the steady axisymmetric basic thermocapillary flow. This trend is similar to the numerical results of Sim and Zebib [33] although the heating direction is reversed.

4.3 HTW in a rotation pool

In the non-rotating pool, according to the analysis by SD [11] and our previous numerical simulations [30], propagation direction of HTW is either in the clockwise or anticlockwise. Both cases should appear in equal probability. However, the present numerical simulations in a rotating pool over a whole range of Ma values ranging between 8.76×10^3 and 2.0×10^4 indicate that the HTW propagate in the opposite direction to the pool rotation, as shown in Fig.8-a and 8-b. This feature is confirmed by some simulations. A simulation was conducted using an artificial HTW patterns propagating in the same direction as the pool rotation. After some calculation time, the propagation direction was reversed. If the pool rotation direction is reversed, the HTW also changes its azimuthal propagation direction. As mentioned in the previous section, pool rotation induces an azimuthal velocity component. Due to this additional azimuthal velocity component of the basic flow, the steady axisymmetric basic thermocapillary flow becomes less stable against a HTW-type disturbances propagating in the opposite to the pool rotation, i.e., HTW propagating opposing to the azimuthal velocity.

The result under a condition of Ma=1.34×10^4 (ΔT=8.0 K) and Ta=0.322 shows a sudden increase of the azimuthal wave number m up to 54 from m=30 for $Ma\leq1.0\times10^4$, as shown in Fig.9. In this case, thick heavy short arm-like patterns appear near the inner

wall and they tend to break up into two thinner curved arms. Let us name them as finger-like arms. Break up occurs at almost 2/3 of the thick wave patterns. The total wave number of the thicker patterns near the inner wall is m=32 on the other hand, m=54 in the outer region. However, the frequencies of the local temperature oscillation measured at those two regions show no difference. Then the phase velocity of the inner waves is larger than that of the outer waves by a factor of $\omega_{inner}/\omega_{outer}$=54/32=1.69. Due to the difference in the phase velocity between the inner and outer waves, the finger-like breakings of the thicker arms are not steady but propagate in the azimuthal direction repeating alternate break-up and recombination as seen in Fig.9a. After one finger-shape wave separates into two thin long waves, the preceding one quickly catches up and gradually links to the preceding thick arm. After a very short time of traveling, a reassembled finger-shape wave comes out again. At the same time, Fig. 9-b (STD) indicates there is a third group of HTW with m=18 propagating along anticlockwise direction.

For a condition of Ma=2.0×10^4 (ΔT=12.0 K) and Ta=0.322, the azimuthal wave number m of HTW dominated in the pool slightly decrease to 48 (Fig.10a). STD (Fig.10b) indicates another HTW group of m= 5 traveling in the anticlockwise direction, although indistinguishable in Fig.10a.

The azimuthal wave number, propagation phase velocity of the HTW and their critical conditions in the rotating and non-rotating pools are summarized in Fig.11. In most cases, the azimuthal wave number increases and the phase velocity $|\omega|$ decrease by the pool rotation when Ma ranged from 8.76×10^3 to 3.0×10^4.

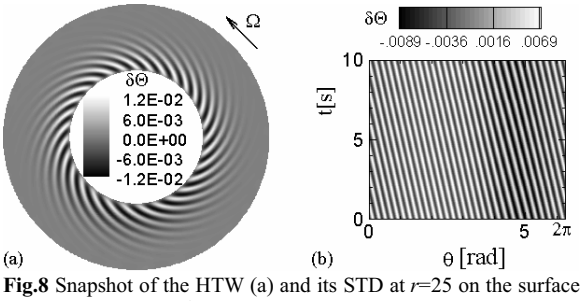

Fig.8 Snapshot of the HTW (a) and its STD at r=25 on the surface (b) when Ma=1.0×10^4(ΔT=6.0K) and Ta=0.322. m=30.

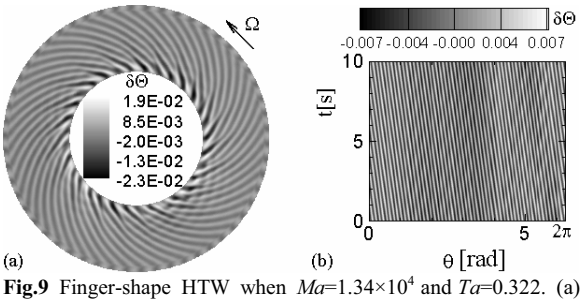

Fig.9 Finger-shape HTW when Ma=1.34×10^4 and Ta=0.322. (a) Snapshot of HTW, m=54 for dominant group, m=32 for inner group and m=18 for fading group traveling along anticlockwise direction. (b) STD on a circle with radius r=30 on the surface.

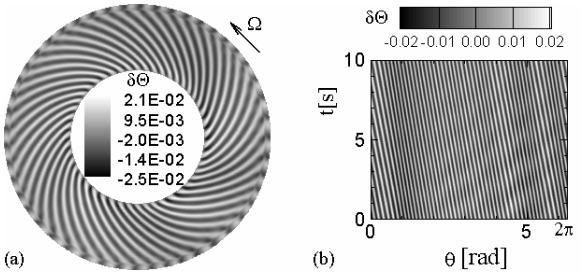

Fig. 10 Snapshot of the HTW (a) and its STD at r=25 on the surface (b) when Ma=2.0×10^4 (ΔT=12K), Ta=0.322.

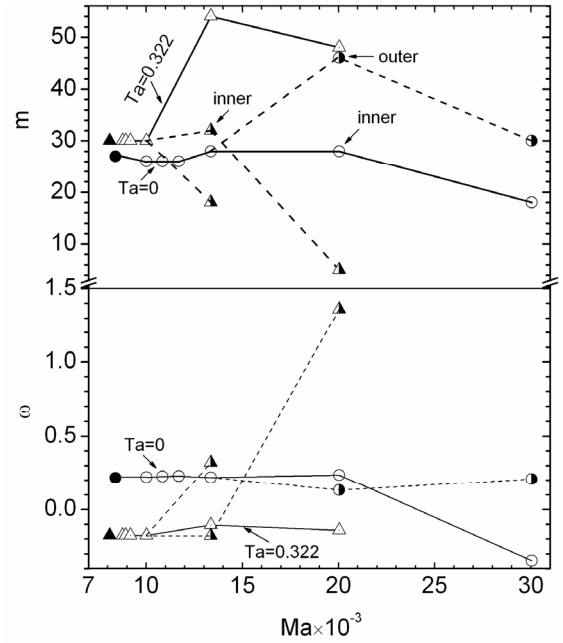

Fig. 11 *Ma* dependencies of wave number m and phase velocity of the HTW in rotating and non-rotating pools. The half filled marks correspond to another group of the HTW. The solid marks correspond the critical conditions.

5. Conclusions

Details of the three dimensional oscillatory thermo-capillary flow in a shallow annular pool (R_i=20 mm, R_o=40 mm and depth d=1.0 mm) of silicone oil (0.65 cSt, Pr=6.7) heated from the outer wall and cooled at the inner wall, were investigated by numerical simulation. In non-rotating annular pool, the critical conditions for the incipience of HTW was determined to be Ma_c= 8.396×10^3, m_c=27 and ω_c=0.217. At slightly super critical conditions, a single group of HTW propagating in the azimuthal direction becomes dominant after very long calculation time. At larger Ma, several groups of HTW with different wave numbers and different propagation directions coexist in the pool.

In a rotating pool at a rate of Ta=0.322, the basic 2-D steady flow becomes less stable against 3-D oscillatory disturbances propagating in the opposite

direction to the pool rotation. The critical conditions are determined as Ma_c=8.096×10^3, m_c=30 and ω_c= -0.176. With *Ma* from 8.76×10^3 to 2.0×10^4, numerical simulations indicate that the HTW always propagates in the direction opposite to the pool rotation. This is caused by the azimuthal component of the basic flow induced by the Coriolis force. The result at *Ma*=1.34×10^4 showed significant increase of wave number up to *m*=54 in the outer region. The finger-shaped patterns appear near the inner wall, this is caused by the instability of wave pattern near the inner wall. The result at *Ma*=2.0×10^4 showed two groups of HTW with different wave numbers, i.e., *m*=48 propagating in the clockwise direction and *m*=5 propagating in the clockwise direction.

Numerical results indicate that the pool rotation destabilizes the basic steady axisymmetric thermo-capillary flow. At *Ta*=0.322 the critical temperature difference is decreased about 3.6% from that for non-rotating case.

References

1) R. Marek, J. Straub, Int. J. Heat Mass and Transfer, **44**, pp.619-632, 2001.
2) C. Reynard, M. Barthes, R. Santini and L. Tadrist, Experimental Thermal and Fluid Science, **29**, pp.783-793, 2005
3) C. Buffone, K. Sefiane and W. Easson, Physical Review E, **71**, pp.1-8, 2005
4) P. Carles, A. Cazabat, J. Colloid and Interface Science, **157**, pp.196-201, 1993.
5) C. E. Chang, W. R. Wilcox, Int. J. Heat and Mass Transfer, **19**, pp. 355-366, 1976.
6) D. Scwabe, A. Scharmann, F. Pleisser, R. Oeder, J. Crystal Growth, **43**, pp. 305-312, 1978.
7) D. C. Miller and T. L. Pernell, J. Crystal Growth, **58**, pp.253-260, 1982.
8) K. -W. Yi, K. Kakimoto, M. Eguchi, M. Watanabe, T. Shyo and T. Hibiya, J. Crystal Growth, **144**, pp. 20-28, 1994.
9) K. Kakimoto, H. Ozoe, Computational Materials Science, **10**, pp.127-133, 1998.
10) T. Azami, S. Nakamura, M. Eguchi, T. Hibiya, J. Crystal Growth, **233**, pp. 99-107,2001.
11) M. K. Smith, S. H. Davis, J. Fluid Mech., **132**, pp.119-144, 1983.
12) F. Daviaud, J. M. Vince, Phys. Rev. E, **48**, pp.4432-4436, 1993.
13) R. J. Riley, G. P. Neitzel, J. Fluid Mech., **359**, pp.143-164, 1998.
14) J. Burguete, N. Mukolobwiez, F. Daviaud, N. Garnier, A. Chiffaudel, Physics of Fluids, **13**, pp.2773-2787, 2001.
15) M. A. Pelacho, J. Burguete, Phys. Rev. E, **59**, pp.835-840, 1999.
16) B. Ezersky, A. Garcimartin, H. L. Mancini, and C. Perez-Garcia, Phys. Rev. E, **48**, pp.4414-4422, 1993.
17) Y. Kamotani, S. Ostrach and A. Pline, Physics of Fluids, **6**, pp. 3601-3609,1994.
18) Y. Kamotani, S. Ostrach and J. Masud, Int. J. Heat and Mass Transfer, **42**, pp.555-564, 1998.
19) Y. Kamotani, Adv. Space Res., **24**, pp. 1357-1366, 1999.
20) N. Mukolobwiez, A. Chiffaudel, F. Daviaud, Phys. Rev. Letters, **80**, pp.4661-4664, 1998.
21) D. Schwabe, U. Moller, J. Schneider, A. Scharmann, Phys. Fluids A, **4**, pp.2368-2381, 1992.
22) S. Hoyas, H. Herrero, A. M. Mancho, Phys. Rev. E, **66**, pp.057301-1-4, 2002.
23) S. Hoyas, H. Herrero, A. M. Mancho, J. Phys. A: Math. Gen., **35**, pp.4067-4083, 2002.
24) N. Garnier, A. Chiffaudel, The European Phys. J. B, **19**, pp.87-95, 2001.
25) D. Schwabe, S. Benz, Adv. Space Rec. **29**, pp. 629-638, 2002.
26) D. Schwabe, A. Zebib, B-C. Sim, J. Fluid Mech., **491**, pp. 239-258, 2003.
27) J. Xu and A. Zebib, J. Fluid Mech., **364**, pp. 187-209, 1998.
28) B. C. Sim, A. Zebib, D. Schwabe, J. Fluid Mech., **491**, pp. 259-274, 2003.
29) Y. R. Li, L. Peng, Y. Akiyama, N. Imaishi, J. Crystal Growth, **259**, pp.374-387, 2003.
30) W. Y. Shi, N. Imaishi, J. Crystal Growth, **290**, pp.280-291, 2006.
31) A. Zebib, Physics of Fluids, **8**, pp.3209-3211, 1996.
32) H. F. Bauer, W. Eidel, Heat and Mass Transfer, **34**, pp.79-90, 1998.
33) B. C. Sim, A. Zebib, Physics of Fluids, **14**, pp.225-231, 2002.
34) J. P. Van Doormaal, G. D. Raithby, Numerical Heat Transfer, **7**, pp.147-163, 1984.
35) H. A. Van Der Vorst, SIAM J. Sci. Stat. Comput., **13**, pp. 631-644, 1992.
36) W. Y. Shi, M. K. Ermakov, N. Imaishi, J. Crystal Growth, in press.